AIAA 99-0682

Determination of Anelastic-Induced Error in Wind Tunnel Test Force and Moment Measurements

Frank W. Steinle Jr.
Sverdrup Technology, Inc., AEDC Group
Arnold Engineering Development Center
Arnold Air Force Base, Tennessee 37389

Dennis Booth
MicroCraft Force Measurement Systems
San Diego, California

Ray D. Rhew
NASA Langley, Hampton, Virginia

37th AIAA Aerospace Sciences Meeting & Exhibit
January 11-14, 1999 / Reno, NV

Determination of Anelastic-Induced Error in Wind Tunnel Test Force and Moment Measurements*

Frank W. Steinle, Jr.†
Sverdrup Technology, Inc., AEDC Group
Arnold Engineering Development Center
Arnold Air Force Base, TN 37389

Dennis Booth
MicroCraft Force Measurements Systems
San Diego, CA

Ray Rhew
NASA Langley
Hampton, VA

Abstract

MicroCraft Inc. performed a specialized calibration of the NASA Langley 104B balance (fabricated from CVM 200 alloy) in their Automatic Balance Calibration System (ABCS) machine to identify and determine the magnitude of anelastic effects in the calibration results. The results analyzed thus far are for the axial-force gage. These results show that anelastic effects for the balance in question are substantial enough to consider revising calibration methodology for situations where highest accuracy is needed. Worst case effects found thus far are of the order of 0.1 percent balance gage capacity. Modeling of the anelastic relaxation process with time constants that are linear with stress level was successful in reducing the uncertainty by at least 50-percent.

Introduction

The wind tunnel testing community has generally accepted the desirability of being able to measure forces and moments accurately enough to support definition of drag coefficient accurate to within one count (0.0001). The two dominant items affecting the ability to measure drag with sufficient accuracy is the measurement of angle of attack to better than 0.01 deg and axial force to better than 0.1 percent of rated capacity of the balance. Gains in accuracy of both measurements are being sought. Optical methods for angle-of-attack measurement are coming into use, as are corrections to accelerometer-based angle measurements for inertial effects. As for balances, uncertainty is generally thought to be of the order of 0.2 to 0.25 percent of capacity. Although it may actually be worse because of bias that results from noncalibrated factors such as temperature, anelastic effects (hysteresis), and inertial effects. Opportunity for improvement includes calibration for these effects, new materials, and new methods of sensing forces and moments such as optical-based methods (birefringent materials and doped optical fibers with either Bragg, or long-wave grating.) This paper reports on progress in accounting for anelastic effects in the relationship between applied forces and moments and strain-based voltage output. Steinle[1] examined the application of the fundamental relationship involving stress, strain, and their respective time-derivatives presented by Zener[2] to the anelastic calibration of the axial-force gage of a 1.1-in., 13-8 PH stainless steel balance. Zener's relation is:

$$\sigma + K_1 \frac{\partial \sigma}{\partial t} = C\left[\varepsilon + K_2 \frac{\partial \varepsilon}{\partial t}\right] \qquad (1)$$

Here, σ, ε, and C represent stress, strain, and modulus, respectively, and K_1 and K_2 are time constants. Zener used "C" for modulus instead of the traditional "E" for Young's modulus. Zener's convention is retained since it may prove necessary to model "C" as a function of strain and/or temperature in the future to reach a more robust model of the anelastic process. Equation (1) with "C" being a constant can be solved in integral form for either stress, given strain as a function of time, or vice-versa. This was done in Ref. 1, with stress assumed proportional to force and strain proportional to output voltage. Equation (2) is the resulting integral expression for strain as a function of stress:

* The research reported herein was performed by the Arnold Engineering Development Center (AEDC), Air Force Materiel Command. Work and analysis for this research were performed by personnel of Sverdrup Technology, Inc., AEDC Group, technical services contractor for AEDC. Further reproduction is authorized to satisfy needs of the U. S. Government.

† Associate Fellow, AIAA.

$$\varepsilon_\tau = e^{-\frac{\tau}{K_2}}\left[\frac{1}{CK_2}\int_{\tau_0}^{\tau} e^{\frac{t}{K_2}}\sigma\left(1-\frac{K_1}{K_2}\right)dt + e^{\frac{\tau}{K_2}}\left(\frac{K_1\sigma_{\iota}}{CK_2}\right)\right. \quad (2)$$

$$\left. - e^{\frac{\tau_0}{K_2}}\left(\frac{K_1\sigma_0}{CK_2}\right) + \varepsilon_{\iota_0} e^{\frac{\tau_0}{K_2}}\right]$$

If the time base (τ_0) is started from the point where stress can be approximated by a constant value, then Equation (3) simplifies to:

$$\varepsilon_\tau = \frac{\sigma_{\tau_0}}{C}\left(1 - e^{-\frac{(\tau-\tau_0)}{K_2}}\right) + \varepsilon_{\tau_0} e^{-\frac{(\tau-\tau_0)}{K_2}} \quad (3)$$

where ε_{τ_0}, with initial values of ε and $\sigma = 0$, can be found from Equation 1.1 by integrating from 0 to τ_0 to result in:

$$\varepsilon_{\tau_0} = e^{-\frac{\tau_0}{K_2}}\left[\frac{1}{CK_2}\int_0^{\tau_0} \varepsilon^{\frac{t}{K_2}}\sigma\left(1-\frac{K_1}{K_2}\right)dt + e^{\frac{\tau_0}{K_2}}\left(\frac{K_1\sigma_0}{CK_2}\right)\right] \quad (4)$$

From Eqs. (2) and (3), it is seen that with Zener's formulation, the amount of anelastic strain can be normalized by the amount of stress. This means that, regardless of the amount of stress, strain-based instrumentation will thus experience the same percentage of error, independent of the working stress level of the balance. Material properties that result in the time constants are the key to reduction of anelastic effects.

In Ref. 1, the relaxation process taking place in the 1.1-in. balance for constant load was best described by two modes (two time constants required instead of just K_2) that differed by roughly an order of magnitude (nominally 100 sec and 1000 sec.) Zener's equation was easily modified to produce an additional relaxation term. The reason for the two-mode representation was not identifiable. Time constants for the magnitude of the load (absolute value) increasing were found to be somewhat different for magnitude reducing. The results showed that the hysteresis loop uncertainty could be reduced by over 84 percent. The reader is referred to Ref. 1 for details. These results were quite encouraging. However, further development was clearly indicated before a viable calibration technique for a six-component balance could emerge from this line of work.

This present study investigated the magnitude of anelastic effects that might be present in results from a typical longitudinal aerodynamic test series performed in the AEDC 16T wind tunnel and applied the method to reduce anelastic error. The balance used is the NASA Langley 104B balance. Figure 1 is a sketch of the 104B Balance. Details of the balance. The approach taken in this study was to perform a self-consistent calibration of the 104B balance in the MicroCraft Force Measurement Systems ABCS machine. The study was accomplished by first checking the machine's load cells for anelastic effects and then performing a series of calibrations of the balance. This series started with a standard calibration, followed by a time-correlated calibration of the balance that followed a load profile over the time period representative of an entire start-run-stop series from a test of a low aspect-ratio aircraft configuration at high subsonic speeds. Unlike the wind tunnel load versus time profile, this series of loads was applied at approximately constant intervals of time. Three time periods were employed. Two of these time periods produced a total time interval representative of the wind tunnel test (90 and 99 minutes.) The third time period (40 minutes) resulted from the ABCS operating at its standard rate. The series finished with a check of the relaxation characteristics of the 104B balance at constant load with both load applied and with load removed.

NASA LaRC Balance NTF-104B

The NASA LaRC NTF-104B was constructed for use in Langley's National Transonic Facility in 1993. The design is based on LaRC standard practices outlined in Ref. 3. An outline drawing that provides the balance's physical characteristics, minus strain gages and wiring, is shown in Fig. 1. In addition, the balance full-scale load capacities, combined, are listed in Fig. 1.

The balance material is VascoMax 200 type C that was heat-treated to a Rockwell C of 42-45. This material is utilized for all of the NTF series balances because of its toughness characteristics at cryogenic temperatures. The balance-to-model interface is a cylindrical fit that must duplicate the fit of a ring and plug gage set. A dowel pin, typically

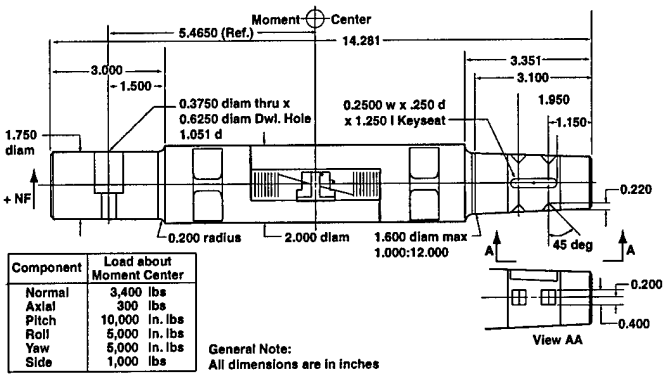

Component	Load about Moment Center
Normal	3,400 lbs
Axial	300 lbs
Pitch	10,000 in. lbs
Roll	5,000 in. lbs
Yaw	5,000 in. lbs
Side	1,000 lbs

Figure 1. NASA Langley 104B balance.

a 0.0002-in. interference fit, secures the balance to the model and defines its location. The sting end attachment is tapered with a key and set screw flats for positioning and securing.

SK 350-ohm type strain gages from Micro Measurements Group, along with their M610 adhesive, are utilized on the balance. Current procedures for installing strain gages on cryogenic balances are detailed in Ref. 4 (balance NTF-104B varies from these procedures in some areas due to the time it was strain gaged in 1993). One variation is the moisture-protective coating. The 104B has a Teflon-based coating that has been repaired with Mcoat B, a Micro Measurements Group Nitril rubber based compound. (Note: NTF-104B is in need of being refurbished to NASA LaRC's new strain gaging standards developed since 1993.) The balance also contains three temperature sensors, thermocouples. They are located at three stations along the balance length, forward, middle, and rear. These are used to monitor balance temperatures and gradients during calibration and wind tunnel testing.

Calibration of the NTF-104B in LaRC's manual calibration stand in 1993 generated the following accuracy results at room-temperature conditions (two-standard deviation accuracy was determined from back calculated loads versus applied loads).

Normal	0.14%
Axial	0.23%
Pitch	0.15%
Roll	0.16%
Yaw	0.11%
Side	0.28%

Reference 5 discusses LaRC's calibration methods.

Anelastic Calibration Test Description

MicroCraft ABCS Machine & Load Cells

The ABCS is the primary calibration system for internal balances at MicroCraft Force Measurement Systems in San Diego, CA. The ABCS (Fig. 2) is a fully self contained and integrated 6-deg-of-freedom calibration system. Figure 2a is a photograph of the overall ABCS, and Fig. 2b is a close-up view of the load adapter rig. The load cells used to sense applied loads are clearly visible. The system is capable of performing all tasks required for the balance calibration process. The machine applies a force to the balance using hydraulic actuators. Precision load cells and high-resolution optical sensors are used to determine applied load vector magnitude and direction. Load

a. Overall system

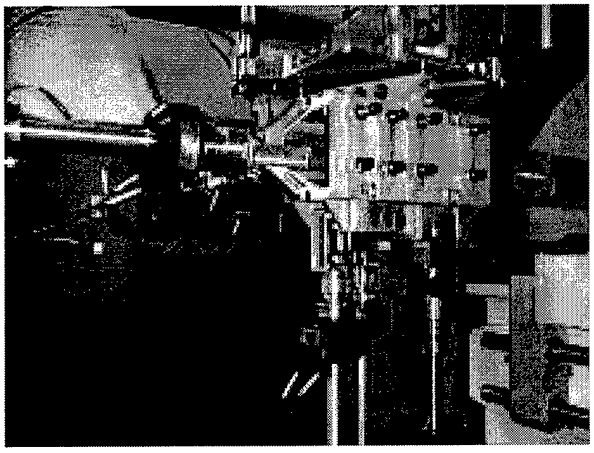

b. Load adapter

Figure 2. Automatic Balance Calibration System.

position is determined from mechanical measurements. The ABCS is based on a non-repositioning principle. The applied force actuators are allowed to move as a result of balance deflection. The position of the deflected balance is measured relative to the fixed end of the balance axis using six, 0.5-micron incremental optical linear displacement gages. By measuring this deflection, the applied force vectors may be established mathematically. The ABCS is essential to the full characterization and calibration of multicomponent balances. The ABCS can apply single and multicomponent loads in any combination within a balance's defined load limits.

Load Cell Calibration Procedure

Prior to using the load cells in the ABCS system, each cell was calibrated to determine primary sensitivities, linearity, and anelastic characteristics. Since the anelastic characteristics are time based, each load cell was loaded to its maximum as quickly as possible. Once full-scale load was reached, load cell output was monitored at specified time intervals. Table I shows the data interval schedule. In all, data were recorded over a 30-min window at full load. Once completed, the weight was removed from each load cell and the same data interval schedule was repeated at zero load conditions (recording relaxation). This process was repeated for both tension and compression on each load cell.

Table I - Data Interval for Load Cell Calibration

Beginning Time	Ending Time	Data Interval
0	1 minute	5 seconds
1 minute	5 minutes	30 seconds
5 minutes	10 minutes	1 minute
10 minutes	30 minutes	5 minute

Balance Calibration Process

The calibration process was accomplished using both the ABCS and manual calibration procedures. Balance matrix coefficients were determined for a variety of matrix models using both ABCS and manual data. The anelastic static loading was completed using dead weight for the application of a three- component load over the same time variable used during the load cell calibrations.

The ABCS calibration process included combinations of two-component loadings to full-scale balance loads. Both a 6x27 and a 6x96 calibration matrix were derived from this calibration data. A second calibration, also using two component loads, was completed to a reduced loading range designed to match the maximum loads typically achieved during wind tunnel testing. The balance was also loaded to full scale using an 837-point loading schedule. This load schedule was selected as representative of the standard calibration that is preformed on this balance. The 837-point schedule applies loads in a different combination to define the balance's characteristics. The balance was then loaded using a calibration schedule representative of actual load conditions recorded during a wind tunnel test. The loads were applied over the same time as that of the test. Five complete calibrations of the test condition-loading schedules were performed, with the fourth schedule run at the standard speed setting on the ABCS. The balance was also loaded manually with dead weights to verify the matrix produced by the ABCS calibration. Over the course of three days, a total of 6200 loading points were applied to the balance.

Analysis of Test Results

Load Cell Anelastic-Relaxation Time-Constant Calibration

If a linear relation between stress in the load cell and applied load is assumed along with a linear relation between strain sensed by the bridge system of the load cell and output voltage, Equation (3) for constant load can be rewritten as:

$$V_\tau = KF_{\tau_0}\left(1 - e^{-\frac{(\tau-\tau_0)}{K_2}}\right) + V_{\tau_0} e^{-\frac{(\tau-\tau_0)}{K_2}} \qquad (5)$$

where V represents the normalized output voltage (millivolts/volt), K is the cell calibration constant relating force to millivolts/volt, and F represents the applied calibration force. The constants K, K2, and V_{τ_0} were determined from a least-squares fit of the test results. The change in output due to anelastic effects is then $KF_{\tau_0} - V_{\tau_0}$. Application of Eq. (5) required interpretation to remove outliers attributed to noise in the output. Weight pan motion and ground vibration and/or air pressure variation

resulting from commercial aircraft operations nearby inducing motion in the building's calibration support structure are thought to have been a factor in the noise that seemed to be present in the test results. The calibration test was not equipped to detect such accelerations by independent means. It should be noted that a milli-g of vertical acceleration would induce a noise spike in the test results of approximately 0.1 percent of applied load. This value of noise is an order of magnitude above the floor noise level sought. With these caveats, it appeared that the load cells used in the ABS machine are very good and have hysteresis that is not statistically significant. Results from the load cell calibration were therefore not used in the analysis and are not given herein.

Balance Anelastic Relaxation Time-Constant Calibration

Difficulties with the method used to determine the relaxation time constants are associated with noise in the data (predominantly inertial effects), change in applied force due to relaxation, and interaction factors due to multicomponent balance loading. The procedures employed to deal with these difficulties required developing a model of the process and then utilizing regression to determine constants in the model. The methodology used to compensate for the above difficulties is as follows:

Inertial Effects. As above, judgment was employed to remove what was considered spurious data by treating them as outliers and removing them through regression analysis. To accomplish removal of outliers, a least-squares fit of the error process was used to provide an initial estimate that was then manually examined to identify outliers, and a final least-squares fit of the results was obtained.

Change in Applied Force. Relaxation effects changing the applied load vector during the anelastic relaxation manual loading are modeled. Because of the loading approach taken which produced a combination of axial-force, normal-force, and pitching-moment loading, relaxation in pitch angle results in a time variation of applied load. A variation of angle within 0.01 deg pitch angle change could not be sensed with the available instrumentation. Since deflection change due to relaxation was expected to be less than 0.01 deg, output of the angle-of-attack sensor was not monitored. Determination of pitch angle to the order of 0.001 deg is needed. The total elastic deflection of the balance due to the loading is estimated at 0.4 deg (based on deflection information from the ABCS calibration.) Assuming an anelastic effect of the order 0.1 percent of balance capacity, this would lead to a change in angle of 0.0012 deg, which is not detectable through either the angle sensor used or regression analysis and hence, is not considered important in the analysis of results. Nevertheless, it was modeled, checked by regression, and found to not be statistically significant.

Time Constant Determination. Assuming that relaxation in pitch angle is negligible, only relaxation at constant stress in the balance flexures is required. Since the balance is homogenous, the time constant associated with all gages of the balance is the same for the same conditions of strain and temperature. This also includes pitch angle relaxation since the balance elastic properties that produce strain also result in rotation. The relaxation is expected to be different for load being applied as opposed to load being removed. Examination of the anelastic loading results indicates that this is the case. Inertial effects appear to dominate the axial-force relaxation at constant load; hence, it was not possible to extract a meaningful time constant from the axial-force load relaxation with load applied. However, the normal-force relaxation results were affected much less, and use of Eq. (5) resulted in a time constant value of nominally 565 sec for applied load. A time constant of 480 sec produces a reasonable fit of the data for both the normal-force and axial-force gages for relaxation after load is removed. The relaxation fit of the data for both gages is shown in Fig. 3. All data points taken are included. The difference in character between the axial-force loading shown in Fig. 3a, as compared to the normal-force loading in Fig. 3b can be seen. The time constant numbers indicated should not be construed as absolute since the noise in the data makes it impossible to determine the time constant within a close tolerance. A better set of laboratory conditions and additional instrumentation is expected to produce better results.

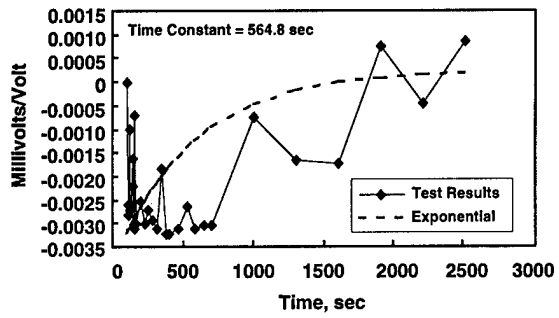

a. Axial force, load applied

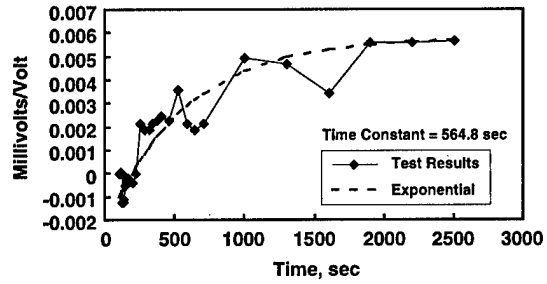

b. Normal force

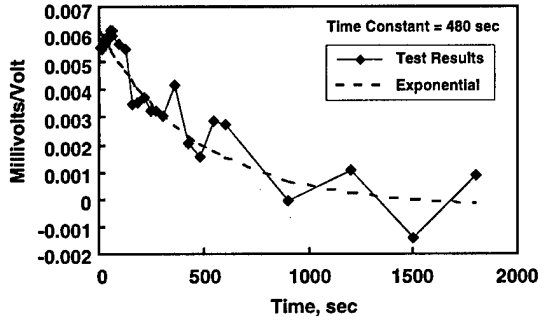

c. Axial force, load removed

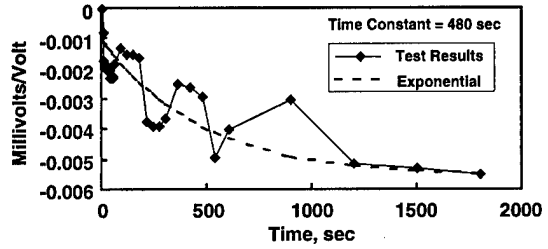

d. Normal forcre, load removed

Figure 3. relaxation time constant determination.

However, the results indicated are quite sufficient for the purpose intended.

There is an inherent assumption in this process that the relaxation constants are the same, regardless of the strain (or stress) level. If the constants are not, then that variation must be modeled sufficiently well, and the above results only give a value appropriate to the strain state of the material. Furthermore, the relaxation constants probably are a function of temperature as well. The experiment reported herein was at constant temperature and thus could not provide any information suggestive of the significance of temperature on relaxation. As will be seen later, modeling of the relaxation process under general loading has led the authors to the conclusion that a higher-order modeling of relaxation constant behavior as a function of stress is needed to match the results of this investigation. A linear model of time constant versus strain (or stress) was proven to be necessary, but not sufficient to capture the entire nature of observed results.

Investigation of Criticality of Load vs. Time. Application of the same load schedule utilizing sufficiently different time intervals indicative of the difference between calibration machine and wind tunnel data acquisition rates will show whether or not time is a significant factor in balance calibration. The procedure followed was to perform the "same" ABCS calibration load schedule with two different time intervals between each new load. The complete load series is representative of the entire load cycle experienced in a wind tunnel test cycle from start of the tunnel to stop with the 104B balance. Figure 4 shows the representative load conditions for normal force, pitching moment, and axial force. The load variations are typical of a transonic aircraft test that encompasses early compressible flow with strong leading-edge suction (Polar E)

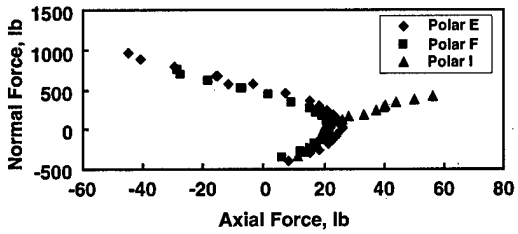

a. Normal force versus axial force

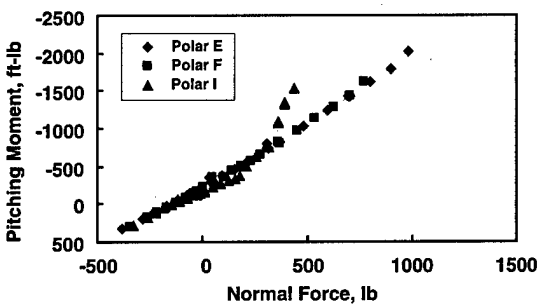

b. Pitching moment versus normal force

Figure 4. Nominal load schedule.

through buffet conditions (Polar I). The range of pitch plane loading conditions approximated a third of the capacity of the balance. The remaining three load components were small and are not shown. Unavoidably, there were small differences between the six components of load being applied at comparable conditions. Thus, it was necessary to correct the output voltage for the difference in load schedule. This was done by multiplying the inverse of a 6X6 calibration matrix times the difference in loading to arrive at a voltage increment to apply to the output generated at the highest rate. It is assumed that after this correction procedure, taking the difference between the two output voltages will remove bias in the calibration results, leaving the relative anelastic effects.

A comparison of the error in calibrated axial force (applied–computed load) is shown in Fig. 5 for the ABCS standard rate (40 min total for 408 data points) against the maximum W.T. load cycle (99 min, total). Output and load cycle output (40 min, total), corrected to the W.T. load cycle, is shown in Fig. 5 for three of the nine polars. Absent anelastic effects, the dominant error should be bias in the calibration that would result in all of the data scattered about a line of agreement with 45-deg slope. As can be seen, this does not occur. There is considerable difference for each of the polars, which is attributed to anelastic effects.

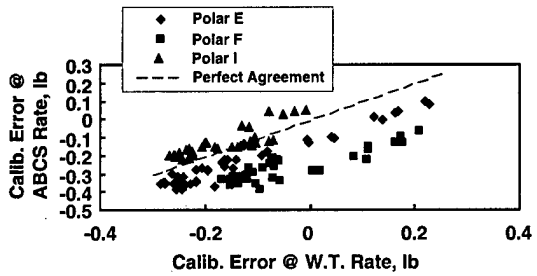

Figure 5. Effect of different load application rates on axial force calibration error.

The error result for each load rate contains the random error difference, plus calibration bias error, plus the difference in anelastic effects between the two load versus time histories. The range of relative anelastic error is substantial. The peak difference is about 0.4 lb which is 0.13 percent of gage capacity. Since the peak loading was about 28-percent capacity, 0.4 lb difference is thus equivalent to 0.46 percent of peak load. Consequently, the variability between the two load rates is 0.23 percent of peak load, which is significant, even though it is only 0.065 percent of gage capacity. Hence, any notion of bias error in the balance calibration results that is based on calibration performed at a high productivity that does not match the wind tunnel load profile productivity could be substantially unrealistic, unless the anelastic effect can be modeled and both the calibration and test results can be corrected. If modeling is not practical, then the obvious approach where higher-than-customary accuracy is needed would be to actually "fly" the balance in an automatic calibration machine that has the capability to vary load versus time in a manner that will closely follow the balance output voltage time-history. The current software controlling the ABCS machine does not permit this type of profile. Conceivably, it is possible to do this with current modern control technology that has learning ability.

Modeling Anelasticity in Calibration Results. Assuming that Eq. (1) essentially represents the physics involved in modeling anelasticity, then it is obvious that some sort of continuous numerical or analog integration process will be required to correct wind tunnel data for anelasticity. In either case, the constants (or variables) K_1 and K_2 must be determined.

Determination of Stress-Rate Constant (K_1). In addition to the relaxation time-constant for constant load (K_2), it is necessary to determine the stress rate constant to be able to represent the anelastic effects. Two different rates of application of load are required to determine this time constant. By modeling the load versus time process, the calibration results discussed above were used regressively to determine the stress-rate constant. The approach taken was to assume that the stress at any location in the balance σ_j is linearly related to the six components of forces and moments, F_i as

$$\sigma_j = \sum_{i=1}^{6} F_i \frac{\partial \sigma_j}{\partial F_i} \qquad (6)$$

Then this result is substituted into a more convenient form of Eq. (2), along with the assumption that output voltage is proportional to strain. Eq. (2)

is integrated by parts to produce a result convenient to discretizing the load-time history:

$$\varepsilon_\tau - \varepsilon_{\tau_0} e^{-\frac{(\tau-\tau_0)}{K_2}} = \frac{1}{C}\left(\sigma_\tau - \sigma_{\tau_0} e^{-\frac{(\tau-\tau_0)}{K_2}}\right)$$

$$-\frac{e^{\frac{-\tau}{K_2}}\tau}{C}\int_{\tau_0} e^{\frac{t}{K_2}}\left(\frac{\partial\sigma}{\partial t}\right)\left(1-\frac{K_1}{K_2}\right)dt \qquad (7)$$

Letting superscript τ represent time and subscript **j** the voltage from gage **j** at time τ, and substituting Eq. (6) into Eq. (7) along with the assumption that each contribution to stress produces a corresponding contribution to voltage through the induced strain, Eq. (8) is obtained:

$$V_j^\tau = \sum_{i=1}^{6} F_i^\tau\left(\frac{\partial V_j}{\partial F_i}\right) - \sum_{i=1}^{6} F_{0_i}^\tau\left(\frac{\partial V_j}{\partial F_i}\right)e^{-\frac{(\tau-\tau_0)}{K_2}} + V_j^{\tau_0} e^{-\frac{(\tau-\tau_0)}{K_2}}$$

$$-e^{-\frac{\tau}{K_2}}\int_{\tau_0}^{\tau} e^{\frac{t}{K_2}}\sum_{i=11}^{6}\frac{\partial F_i}{\partial t}\left(\frac{\partial V_j}{\partial F_i}\right)\left(1-\frac{K_1}{K_2}\right)dt \qquad (8)$$

The partial derivatives of output voltage with respect to force or moment in Eq. (8) are approximated by the linear terms of the inverse calibration matrix. Should there be significant cross-product terms, these terms would also be added. Eq. (8) is in a form that can be converted to finite differences. Assuming that over each interval of time the rate of change of each force can be treated as a constant, Eq. (8) can be integrated:

$$V_j^{\tau_n} = \sum_{i=1}^{6} F_i^\tau\left(\frac{\partial V_j}{\partial F_i}\right) + V_j^{\tau_{n-1}} e^{-\frac{(\tau_n-\tau_{n-1})}{K_2}}$$

$$-\sum_{i=1}^{6} F_i^{\tau_{n-1}}\left(\frac{\partial V_j}{\partial F_i}\right)e^{-\frac{(\tau_n-\tau_{n-1})}{K_2}} \qquad (9)$$

$$-\left(\frac{K_2-K_1}{t_n-t_{n-1}}\right)\left(1-e^{-\frac{(\tau_n-\tau_{n-1})}{K_2}}\right)\sum_{i=1}^{6}\left(F_i^{\tau_n}-F_i^{\tau_{n-1}}\right)\left(\frac{\partial V_j}{\partial F_i}\right)$$

Equation (9) shows that the anelastic effect is embodied in the second through the last term on the right-hand side. Taking the limit as τ/K_2 becomes very large at constant **F**, Eq. (9) reduces to just the first term, which is the true "back-calibration" result with anelastic effects removed. Consequently, during the calibration process, a subtraction of the voltage bias due to anelasticity would produce a data set that can be used to arrive at the correct value for the balance calibration matrix with anelastic effects removed. Owing to the formulation, the predicted anelastic component is coupled to the current estimate of the end result. Consequently, rigorous processing of the calibration results requires iterating the recomputed calibration results back into Eq. (9). Iteration should not be necessary, since the magnitude of the anelastic component is of the order of 0.1 percent of gage capacity. Use of Eq. (9) requires testing to determine whether or not the magnitude of the voltage is greater or less than the fully-relaxed value. If it is greater, then the K_2 value corresponding to decreasing load (e.g., 480 sec at zero load) is required. If it is less, then K_2 equals the value corresponding to increased loading.

Since the true value of voltage with anelastic effects cannot be known unless K_1 is also known, subtracting the result of two identical load schedules performed at different time intervals will thus eliminate the first term on the right-hand side of Eq. (9), including bias. A least-squares approach can then be taken to determine K_1, which will best match the differential anelastic voltage inferred from Fig. 5. The approach taken is to start from the condition of all forces and voltage being zero and then marching forward in time for each data point.

The assumption of constant values for K_1 and K_2 did not prove satisfactory herein. Assuming that the general form of Eq. (1) is a good representation, the next logical approach is to treat K_1 and K_2 as variables. A linear variation with absolute value of strain (or stress) for K_1 and K_2 was assumed:

$$K_1 = K_{01}\left(1 + c_1\left|\frac{\sigma}{C}\right|\right) = K_{01}(1 + c_1|V|) \qquad (10)$$

$$K_2 = K_{02}(1 + c_2|\varepsilon|) = K_{02}(1 + c_2|V|) \qquad (11)$$

The use of the absolute value was chosen because the output of each balance gage is from a full bridge that is subjected to tensile stress in half of the legs of the bridge and compressive stress in the other half. Thus, the change in the output

should not vary with the sign of the stress level. It should vary with whether or not relaxation is increasing or decreasing the absolute value of stress. The rate of change of the relaxation constants is slow enough that they can be treated as constants over each interval of time and updated accordingly. This was accomplished by substituting Eqs. (10a) and (103b) into Eq. (9). Regression to determine the best overall fit of all of the anelastic computed results against the difference in output for the two experiment load rates was performed. The values arrived at are shown in Table II.

Table II. Anelastic Time Constants

Constant	K_{01}	C_1	K_{02}	C_2
Increasing Load	565.9	0.424	564.1	0.424
Decreasing Load	480	0.395	480.1	0.4398

As previously indicated, the corrected result was used in the regression to determine the above final set of constants. Figure 6 shows the comparison of the experimentally determined difference in anelastic results, along with the computational results based on the above constants for the axial-force gage for all nine polars. The polars (A through I) are in the order in which the load was applied. In general, it is obvious that the approach taken is in the correct direction, and it does show promise in that the effect is predicted to a large degree. There are instances, e.g., polars A, D, and E, where the trends predicted are significantly different from the experimental results. This argues for more definitive work, especially in determining material properties from direct measurement.

Figure 7 shows the relative anelastic error for both experiment and computed results sequentially for all polars. The agreement with the general trend shows that in the gross sense, the model captures the trend. A fine detail comparison between experiment and computed results shows that a different model is required to properly capture the true nature of the anelastic effects.

A projection of the absolute level of anelasticity for each of the two loading rates is shown in Fig. 8 for polars E, F, and I. The projection is based on the constants given in Table II. The difference between the two sets of data is then the computed

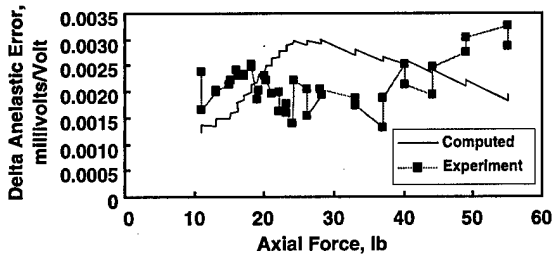

a. Polar A

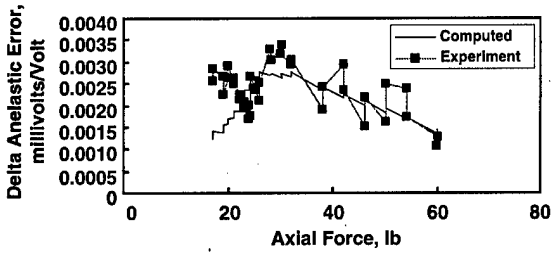

b. Polar B

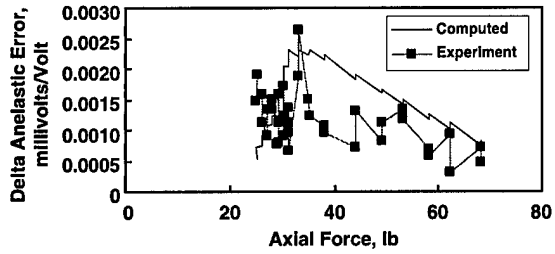

c. Polar C

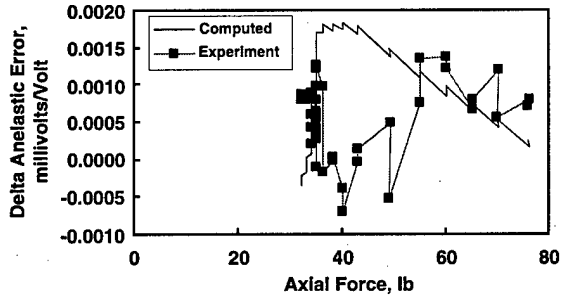

d. Polar D

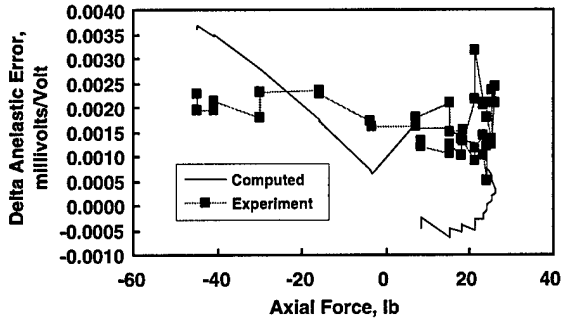

e. Polar E

Figure 6. Comparison of computed on experimental anelastic error due to load rate.

difference in anelasticity for the two load rates. The maximum value of predicted anelastic error is 0.01 millivolts/volt, which is equivalent to 0.19 percent gage capacity! Further work is needed to extract a meaningful estimate of the absolute level of anelasticity in each of the load conditions. One impediment is the lack of definitive knowledge of the timing for each data point. The analysis was performed assuming that each point was taken at the same interval. A further difficulty is associated with the need to do a more careful analysis of the calibration results and extract a first estimate of the anelastic effects from the input data and then reprocess the calibration to try to remove bias error that is not due to anelasticity. This will be tedious at best. On the other hand, the usefulness of the present method for correcting for anelasticity can

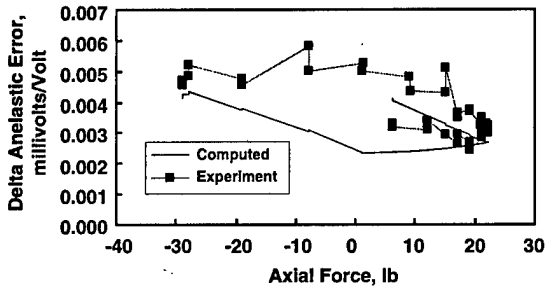

f. Polar F

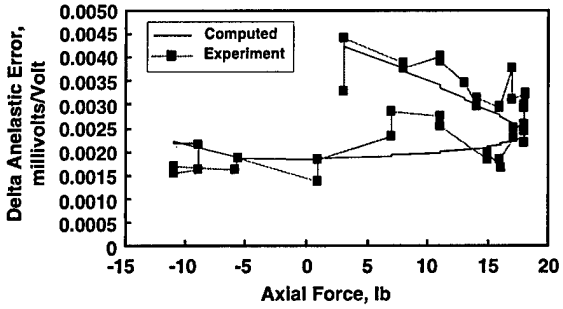

g. Polar G

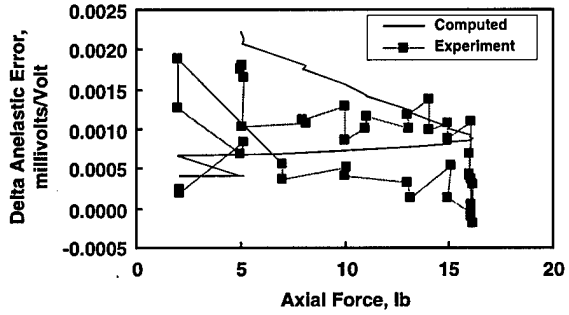

h. Polar H

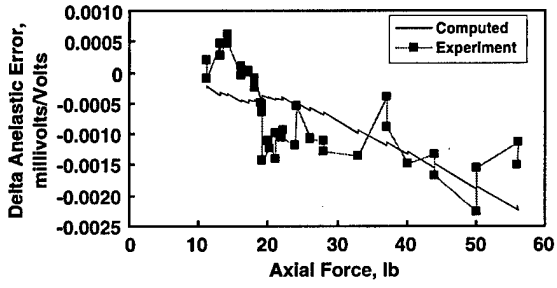

i. Polar I

Figure 6. Concluded.

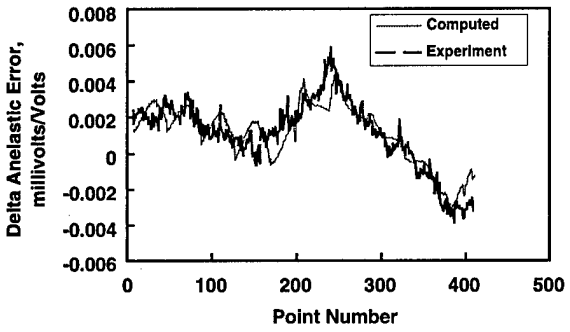

Figure 7. Sequential relative anelastic error.

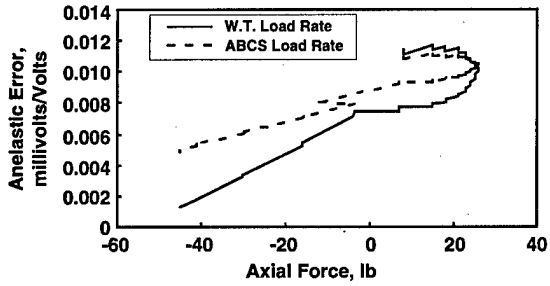

a. Polar E

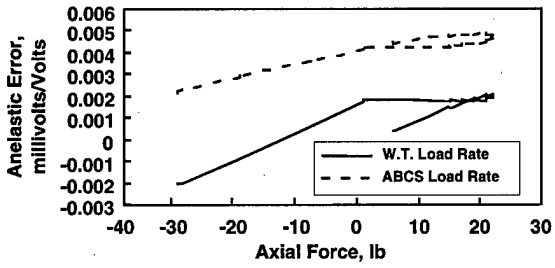

b. Polar F

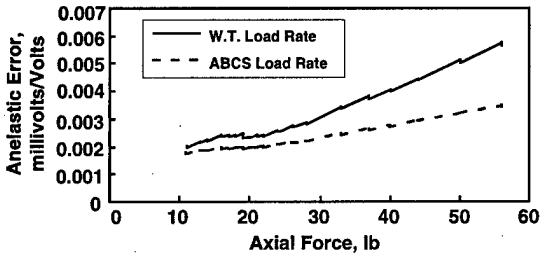

c. Polar G

Figure 8. Predicted anelastic error.

be seen by comparing Figs. 9 and 10. The reduction in relative anelastic error between the two load application rates is seen to be at least 50 percent. Although not conclusive, it does offer promise of obtaining similar results on an absolute basis.

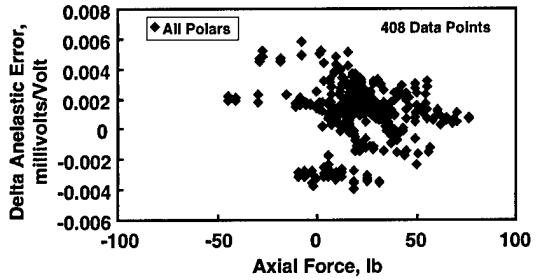

Figure 9. Experimental relative anelastic error.

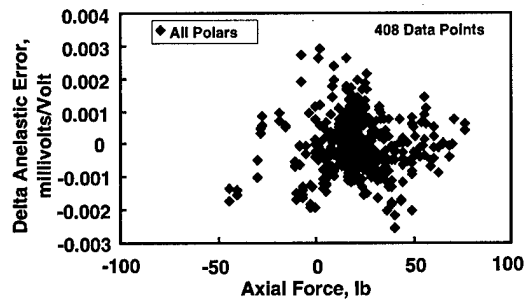

Figure 10. Residual experimental relative anelastic error after computational correction.

Concluding Remarks and Recommendations

1. It is hoped that the result of this work will spark interest in others to join in researching the correction for anelasticity, which shows promise of reducing the uncertainty associated with strain-based measurements of forces and moments. As a first step, it is recommended that a relaxation check be made for balance output under load and with load removed to determine both the magnitude of relaxation and the time constants involved and that any results of such tests be shared with the AIAA GTTC, Balance Calibration Working Group.

2. The comparison of the "same" calibration at different rates should serve as a wake-up call to those who place confidence in the conventional balance calibration result as a faithful replication of the wind tunnel result, absent temperature effects. Verification of the calibration results for a load application rate that matches the wind tunnel test is recommended. Also, it should not have escaped the reader's eye that the anelastic effects are likely to be worse than the difference in anelastic effects shown herein. Considerably more work is warranted, especially direct laboratory measurement of anelastic characteristics under the range of conditions experienced by a balance.

3. The mean value of anelasticity at each data point in the calibration introduces a bias at each load in the calibration process that then results in a nonlinear term being in the gage calibration when there would otherwise not be one. Removal of anelastic effects will then make it possible to establish the true nonlinearity in the calibration, which could result from a number of causes, including the modulus not being a constant and the inherent nonlinearity in a basic strain gauge output. In either case, the current calibration methodology employed to process the post-anelastic correction calibration results will handle those systematic nonlinear effects.

4. Although this paper has not discussed application of the anelastic calibration results to the reduction of wind tunnel data, it does not pose a problem. The basic differential equation still holds, and it is trivial to process the results going from measured voltage to a corrected voltage that can then be used with a standard calibration to arrive at the final result.

5. The success of the present method in reducing apparent anelastic error between two different calibration load time cycles merits further work to develop a calibration technique and the necessary application of anelastic correction to test results and to transition such a technique to routine application. Any efforts toward this effect should be shared with the AIAA GTTC Balance Calibration Working Group.

References

1. Steinle, Frank, "Advanced Balance Calibration Technique for Getting Around the Hysteresis Loop," 88th Semiannual Meeting of the Supersonic Tunnel Association, Nashville, TN, Oct. 19-22, 1997.

2. Zener, Clarence, "*Elasticity and Anelasticity of Metals*," University of Chicago Press, Chicago, Ill., 1948.

3. Rhew, Ray, "NASA LaRC Balance Design Concepts," First International Strain Gauge Balance Symposium, 1996.

4. Moore, Thomas C., "Recommended Strain Application Procedures for Langley Research Center Balance and Test Articles," NASA TM 110327, March 1997.

5. Ferris, Alice T., "An Improved Method for Determining Force Balance Accuracy," ISA Conference Paper #93-093, May 1993.